THE JOURNAL OF PHYSICAL CHEMISTRY A
A JOURNAL OF THE AMERICAN CHEMICAL SOCIETY

pubs.acs.org/JPCA

Article

Experimental Study of the Validity of Entangled Two-Photon Absorption Measurements in Organic Compounds

Samuel Corona-Aquino, Omar Calderón-Losada, Mayte Y. Li-Gómez, Hector Cruz-Ramirez, Violeta Álvarez-Venicio, María del Pilar Carreón-Castro, Roberto de J. León-Montiel,* and Alfred B. U'Ren*

Cite This: J. Phys. Chem. A 2022, 126, 2185−2195

Read Online

ACCESS | Metrics & More | Article Recommendations | Supporting Information

ABSTRACT: Entangled two-photon absorption (ETPA) has recently become a topic of lively debate, mainly due to the apparent inconsistencies in the experimentally reported ETPA cross sections of organic molecules obtained by a number of groups. In this work, we provide a thorough experimental study of ETPA in the organic molecules Rhodamine B (RhB) and zinc tetraphenylporphirin (ZnTPP). Our contribution is 3-fold: first, we reproduce previous results from other groups; second, we on the one hand determine the effects of different temporal correlations—introduced as a controllable temporal delay between the signal and idler photons to be absorbed—on the strength of the ETPA signal, and on the other hand, we introduce two concurrent and equivalent detection systems with and without the sample in place as a useful experimental check; third, we introduce, and apply to our data, a novel method to quantify the ETPA rate based on taking into account the full photon-pair behavior rather than focusing on singles or coincidence counts independently. Through this experimental setup we find that, surprisingly, the purported ETPA signal is not suppressed for a temporal delay much greater than the characteristic photon-pair temporal correlation time. While our results reproduce the previous findings from other authors, our full analysis indicates that the signal observed is not actually due to ETPA but simply to linear losses. Interestingly, for higher RhB concentrations, we find a two-photon signal that, contrary to expectations, likewise does not correspond to ETPA.

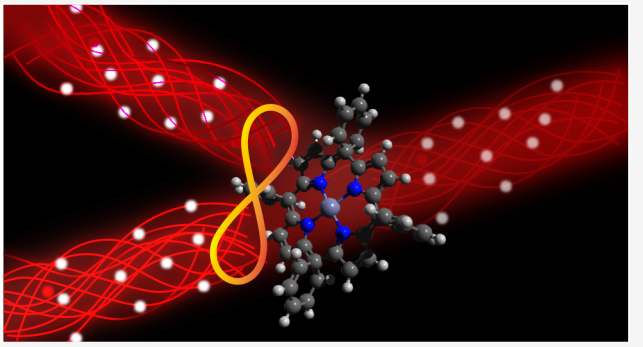

INTRODUCTION

Since its inception in 1931, the work of Maria Goeppert Mayer on two-photon absorption (TPA) has become a fundamental tool for probing processes that require a sharp resolution and high energy density concentrations, as in the case of biological imaging and microscopy.[1] Remarkably, TPA has also improved spectroscopic methods by enabling the study of the symmetry of excited states in organic molecules, including electronic transitions of a system that are normally inaccessible by one-photon absorption (1PA).[2,3]

Despite its broad applicability, TPA is an extremely inefficient process, often requiring 0.01−1 nJ pulse energy to achieve optimal excitation efficiencies.[3−5] This high peak-excitation is required to compensate for the low probability that two photons will reach a molecule nearly simultaneously so as to secure the excitation. The latter, however, can result either in photobleaching due to its dependence on the square of the intensity, or in heating-induced damage.[6,7] Nevertheless, theoretical research developed in the last three decades has presented a promising solution by proposing the use of nonclassical light sources so as to induce the two-photon excitation at considerably lower incident fluxes, leading to the possible use of these sources in delicate systems without causing damage by high incident powers.[8−16] Recent investigations exploit nonlinear processes such as spontaneous parametric down conversion (SPDC) and spontaneous four wave mixing (SFWM) in order to generate entangled photon pairs to be used as source for TPA in a phenomenon referred to as entangled two-photon absorption (ETPA).[17−32] By virtue of the strong correlations between the photons in each pair, the phenomenon has been reported at significantly lower photon fluxes, on the order of 10^{12} photons s^{-1} cm^{-2}, which corresponds to a photon rate of 10^6 pairs/s,[33] representing a clear advantage over classical TPA. However, a detailed analysis is needed in view of recent findings on the improvement achieved on the fluorescence signal using squeezed light over a coherent source in a two-photon

Received: January 28, 2022
Revised: March 18, 2022
Published: April 6, 2022

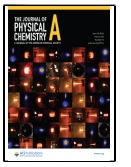

https://doi.org/10.1021/acs.jpca.2c00720
J. Phys. Chem. A 2022, 126, 2185−2195

absorption experiment,[34] where the authors report an enhancement lower than 10^2. This result is in the same direction as in a recent work by Landes et al.[35] in which a thorough analysis of the quantum advantage is carried out for realistic experimental scenarios, showing that while this enhancement could be of several orders of magnitude when compared to a corresponding (classical) TPA experiment, the actual ETPA rates are too low to be observable in typical experiments. Note that if a quantum-enabled advantage of ETPA over classical TPA were to be experimentally confirmed, the resulting low photon flux regime would open up the possibility of performing two-photon spectroscopy with more compact and cost-effective devices.

The absorption cross sections δ_{TPA} and σ_E constitute useful metrics for TPA and ETPA, respectively; the first has typical values on the order of $\delta_{TPA} \sim 10^{-48}$ cm^4 s/photon for most organic molecules.[36] Several investigations have discussed the potential quantum advantage in the ETPA process. This has led to a number of experiments on organic molecules including biological samples, such as proteins,[37] thienoacenes,[38] and commercially available dyes such as fluorescein,[34] zinc tetraphenylporphyrin (ZnTPP) and Rhodamine B (RhB).[25] These experiments have reported ETPA cross sections on the order of $\sigma_E \sim 10^{-18}-10^{-21}$ cm^2/molecule. However, these numbers have recently been challenged by new experimental evidence, based on transmission- and fluorescence-based measurements, that place realistically detectable ETPA cross sections in the range of $10^{-25}-10^{-23}$ cm^2/molecule.[39,40]

An important property of ETPA is its dependence on the temporal delay between the absorbed entangled photons. This dependence is such that the absorption is expected to be suppressed if the photons arrive at the molecule with a temporal delay much larger than the entanglement time, T_e of the photon pairs.[17,19,20] A recent report has shown a possible time dependence on the ETPA signal for Rh6G in ethanol.[41] However, it is worth pointing out that, although the presented behavior is broadly consistent with theoretical predictions, the interferometric scheme used to control the temporal delay introduces a dependence of the incoming photon-pair flux on the delay, i.e., unrelated to the ETPA process, which ultimately influences the ETPA signal.

This possible artifact deserves, without any doubt, a more detailed analysis, particularly in view of a recent work by Landes et al.,[42] in which the authors report no measurable ETPA signal using the same molecular system, and a similar experimental arrangement. Note also that other related works studying the temporal-delay dependence of the ETPA signal have focused on its nonmonotonic behavior[10,26,43] rather than its suppression outside the time-correlation of the absorbed photons.

A recent work by Mikhaylov et al.[44] has drawn attention to the difficulties in discriminating the effects due to ETPA from those resulting from other (linear) phenomena which are not dependent on the temporal delay. Because in that work the introduction of a deterministic delay is not possible; i.e., part of the photon-pair flux always reaches the sample without delay,[45] full ETPA suppression may not be observed directly. One of the main motivations of our work is to perform an ETPA experiment with a deterministic temporal delay introduced between the two photons as a key test of the observed signal. Because of the manner in which the delay is introduced (see below), the photon-pair flux ends up being delay-dependent, as indeed is also the case in ref 41. In our case, there is a factor of 2 difference between the photon-pair flux at zero delay compared to large delay. In our present work, we introduce an analysis that is insensitive, on the one hand, to any linear losses in the system and, on the other hand, is insensitive to the photon-pair flux used and therefore is unaffected by the above factor of 2 difference.

In this work, we aim to assess the viability of the transmission-based scheme, commonly used to measure the ETPA cross-section values of organic molecules. Our setup was designed so that the experimenter can choose one of two configurations: a collinear configuration which permits a direct comparison with previous works[37] and a noncollinear configuration which permits on the one hand the introduction of a temporal delay between the signal and idler photons and on the other hand allows us to compare the purported ETPA behavior with a reference arm that does not contain a sample. In addition, we present a new model that accounts for time-independent effects and therefore effectively estimates the ETPA cross sections. Conveniently, we have selected the organic molecules RhB and ZnTPP for our ETPA experiments, so as to facilitate comparisons with previous works.[25,36,44]

THEORY

It is known that SPDC light exhibits a high degree of correlation so that the detection of one of the photons in a given pair, at a particular space-time location, determines the corresponding location where the detection of its twin is expected.[46] Due to the fact that in a photon-pair stream the presence of any one photon is accompanied by its twin, the probability of excitation of an atom (or molecule) by an individual photon pair is independent of the flux and consequently the two-photon absorption process exhibits a transition rate with a linear dependence on the incident flux.[8]

Let us consider the total number of excited molecules (per unit volume) during an interaction time, T,

$$n_{\mathrm{molec}}^{(2)} \approx \frac{1}{2}\sigma_E \phi T n_0 \tag{1}$$

where σ_E denotes the entangled-photon absorption cross-section of a molecule, $\phi = N_{\mathrm{ph}}/(AT)$ is the photon flux (with N_{ph} the number of incident photons and A the transverse area of the photon-pair spatial mode), and $n_0 = cN_A$ is the density of molecules (with c the concentration and N_A Avogadro's number). As a result, the total number of absorbed photon-pairs, also referred to as biphotons, $N_{\mathrm{ph}}^{(2)}$, in an interaction volume V, is expressed as follows

$$N_{\mathrm{ph}}^{(2)} \approx 2n_{\mathrm{molec}}^{(2)} V = \frac{\sigma_E c N_{\mathrm{A}} V}{A} N_{\mathrm{ph}} \tag{2}$$

Interestingly, from the experimental parameters, we can obtain the following expression

$$\sigma_E = \frac{(N_{\mathrm{ph}}^{(2)}/N_{\mathrm{ph}})A}{cVN_{\mathrm{A}}} = \frac{m}{clN_{\mathrm{A}}} \tag{3}$$

where m is the slope calculated from the linear relationship between $N_{\mathrm{ph}}^{(2)}$ and N_{ph} at different concentrations. Note that the rightmost expression in eq 3 is obtained by approximating the interaction volume, determined by the photon-pair spatial mode, as a cylinder with transverse area A and length $l \leq z_R$, where l is the length of the cuvette which contains the molecules and z_R is the Rayleigh range. For the specific case of a cuvette of $l = 1$ cm length, this approximation is valid if the

https://doi.org/10.1021/acs.jpca.2c00720
J. Phys. Chem. A 2022, 126, 2185−2195

biphoton spatial mode is focused to a spot size with a radius $\gtrsim$36 μm.

Sensitivity of the Transmittance Scheme. In typical transmission-based ETPA measurements, two different signals are needed: a reference signal, which is obtained by probing a cuvette containing the solvent only (R_{solv}), and a second signal, obtained with a solution of the sample under study (R_{samp}), where these two signals are the photon rates (photons/s) passing through each system. The difference between these signals yields the absorption rate (R_{abs}). Because the reference-signal values take into account linear effects produced by the solvent and the cuvette, R_{abs} arguably exhibits only the effects due to the ETPA process.

In what follows, we describe a method for estimating the sensitivity of an instrument that relies on transmission measurements for obtaining ETPA cross sections. Let us define the mean number of photons detected within a time interval Δt as $\bar{N}_\mu = \Delta t R_\mu$, with standard deviation ΔN_μ (where μ corresponds to "solv" or "sam"). Therefore, a statistically significant difference between the signals will occur if

$$\bar{N}_{sam} + \frac{1}{2}\Delta N_{sam} \leq \bar{N}_{solv} - \frac{1}{2}\Delta N_{solv} \tag{4}$$

Note that because our measurement is based on photon counting with Poissonian statistics, each uncertainty corresponds to the square root of the mean value, so that $\Delta N_\mu = \sqrt{\bar{N}_\mu}$. As a consequence, the quantity $b \equiv 1/(2\sqrt{\bar{N}_{solv}})$ serves as a lower bound for the ratio $\bar{N}_{abs}/\bar{N}_{solv}$ (with $\bar{N}_{abs} \equiv \bar{N}_{solv} - \bar{N}_{sam}$),

$$\frac{\bar{N}_{abs}}{\bar{N}_{solv}} \geq \frac{1}{2\sqrt{\bar{N}_{solv}}} \equiv b \tag{5}$$

Using the definition of the cross-section in eq 3, σ_E will be bounded by σ_E^{LB}, i.e., $\sigma_E \geq \sigma_E^{LB}$, with

$$\sigma_E^{LB} = \frac{b}{cIN_A} \tag{6}$$

In a typical experiment using SPDC light,[47,48] $\bar{N}_{solv} \sim 10^5$ photons in a time Δt = 1 s, which implies that the bound is $b \sim 10^{-3}$. This means that for concentrations in the range of tens of μM, the lower bound is on the order of $\sigma_E^{LB} \sim 10^{-19}$ cm^2/molecule, whereas for concentrations in the range of tens of millimolar the lower bound is on the order of 10^{-22} cm^2/molecule.

Biphoton Absorption Rates. In order to obtain a value for the ETPA signal $\bar{R}_{abs}/\bar{R}_{solv} = 1 - \bar{R}_{samp}/\bar{R}_{solv}$, previous works rely on directly computing the ratio $\bar{R}_{samp}/\bar{R}_{solv}$ from the singles or coincidence counts obtained in transmission through the cuvette, containing the sample $\bar{R}_{samp}$ and the solvent only $\bar{R}_{solv}$. This approach, however, can be misleading, as it ignores the various losses throughout the experiment. Therefore, we follow Schneeloch et al.,[49] using a simple model which relies on the actual photon-pair flux expected at the cuvette. Let us assume that $R^{(2)}$ biphotons per second reach the cuvette and, after the ETPA sample, these are separated into two arms by a 50/50 beamsplitter. The resulting photons in each of the two arms are coupled into an optical fiber and detected at a single photon detector. This results in a rate of singles detection for each of the two channels (R_1, R_2) and a coincidence rate R_{12}, expressed as follows

$$R_1 = (\epsilon_1\kappa_1\beta_1)R^{(2)} + \varphi_1 \tag{7a}$$

$$R_2 = (\epsilon_2\kappa_2\beta_2)R^{(2)} + \varphi_2 \tag{7b}$$

$$R_{12} = (\epsilon_1\epsilon_2\kappa_1\kappa_2\beta_{12})R^{(2)} + \varphi_{12} \tag{7c}$$

with the coupling efficiencies being κ_1 and κ_2 for the signal and idler arms, respectively. The linear absorption, detector efficiencies, scattering, and all other losses are taken into account in the transmission efficiencies ϵ_1 and ϵ_2, while the probabilities that the photons in each pair are transmitted, reflected or separated by the beamsplitter are described by β_1, β_2, and β_{12}, respectively (with values $\beta_1 = \beta_2 = {}^3/_4$, and $\beta_{12} = {}^1/_2$). We also incorporate in this simple model the dark-count rate in each of the two detectors (φ_1 and φ_2), as well as accidental coincidence count rate φ_{12}. Note that by combining the set of equations in (7), the biphoton rate that reaches the cuvette can be expressed as

$$R^{(2)} = \left(\frac{\beta_{12}}{\beta_1\beta_2}\right)\frac{\tilde{R}_1\tilde{R}_2}{\tilde{R}_{12}} \tag{8}$$

where the symbols with a tilde represent each of the rates corrected for dark or accidental counts, i.e., $\tilde{R}_\mu = R^{(2)} - \varphi_\mu$, with $\mu \in \{1, 2, 12\}$. Interestingly, because of the structure of this last expression, we are able to correctly estimate the two photon rates $R^{(2)}$, irrespective of linear losses quantified by ϵ_1, ϵ_2, κ_1, and κ_2. Note from eqs 7a–7c, that the effect of ETPA is to reduce the photon-pair rates from $R^{(2)}_{solv}$ to $R^{(2)}_{samp}$, according to $R^{(2)}_{samp} = \epsilon_{ETPA} R^{(2)}_{solv}$, where ϵ_{ETPA} represents the photon-pair rate reduction produced by ETPA.

We can now use eq 8, considering that β_1, β_2, and β_{12} are all independent of whether or not ETPA takes place, to express the ratio of absorbed to incident biphotons as

$$\frac{\bar{R}^{(2)}_{abs}}{\bar{R}^{(2)}_{solv}} = 1 - \frac{\bar{R}^{(2)}_{samp}}{\bar{R}^{(2)}_{solv}} = 1 - \epsilon_{ETPA} = 1 - \frac{\tilde{R}_1^{samp}\tilde{R}_2^{samp}/\tilde{R}_{12}^{samp}}{\tilde{R}_1^{solv}\tilde{R}_2^{solv}/\tilde{R}_{12}^{solv}} = \Gamma \tag{9}$$

From eqs 3 and 9, we may then express the cross-section as follows

$$\sigma_E = \frac{\Gamma}{cIN_A} \tag{10}$$

In the experimental section below we discuss two experiments, one of which involves the introduction of a temporal delay τ between the signal and idler photons prior to reaching the ETPA sample. Because of the specific method used to introduce this delay (based on Hong–Ou–Mandel interference), the available photon-pair rate $R^{(2)}$ depends on τ (specifically, with $R^{(2)}$ at τ = 0 being twice as large as compared to the corresponding value at a large positive or negative delay, see Supporting Information. However, considering that the quantities ϵ_1, ϵ_2, κ_1, κ_2, β_1, β_2, and β_{12} are all delay-independent, any delay dependence of the photon-pair rates, i.e., $R^{(2)} = R^{(2)}(\tau)$, will cancel out in eq 9, thus not affecting the ETPA signal $\bar{R}^{(2)}_{abs}/\bar{R}^{(2)}_{solv}$. Therefore, remarkably, we can use eq 10 to monitor the ETPA signal behavior in the transmission scheme, unaffected by any intrinsic dependence of the incoming photon-pair flux on the delay between the absorbed

https://doi.org/10.1021/acs.jpca.2c00720
J. Phys. Chem. A 2022, 126, 2185–2195

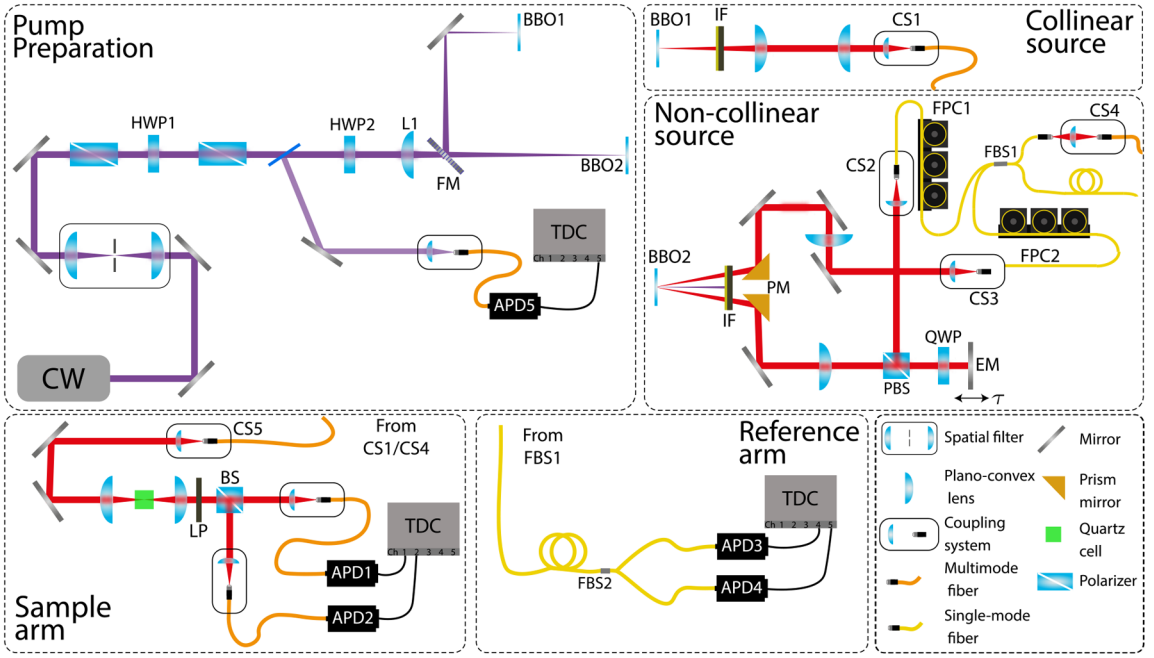

Figure 1. Experimental setup designed to measure the ETPA rate with a transmission-based scheme. Two different experimental configurations were used, based on (i) a collinear SPDC source and (ii) a noncollinear SPDC source, in which two equivalent photon-pair streams with a signal-idler temporal delay τ are obtained through a Hong−Ou−Mandel interferometer. These two photon-pair streams are directed to two detection systems, the sample and reference arms, which allows us to study the ETPA signal in comparison with an equivalent setup without a sample. Note that regardless of the configuration used, the photon-pair stream interacts with the ETPA sample collinearly; in the noncollinear configuration, the signal and idler photons are controllably delayed upon reaching the sample.

photons and/or on any linear loss mechanisms sustained by the photon pairs.

Also note that due to the existing linear relationship between the rates (singles and in coincidence) for solvent and samples, i.e., $R_{\mu}^{\text{samp}} = m_{\mu} R_{\mu}^{\text{solv}}$ (with $\mu = 1, 2, 12$), the biphoton ratio in eq 9 can be calculated using the expression

$$\frac{\bar{R}_{\text{abs}}^{(2)}}{\bar{R}_{\text{solv}}^{(2)}} = 1 - \frac{m_1 m_2}{m_{12}} \tag{11}$$

where each m_{μ} can be obtained by a linear fitting of the corresponding experimental transmission data.

METHODS

As stated above, our experimental design incorporates two distinct configurations, which can be selected by the experimenter, based either on a collinear or a noncollinear, frequency-degenerate SPDC source. In both cases, a continuous wave (CW) laser centered at 405 nm is used as a pump for the SPDC process, as shown in the pump preparation stage in Figure 1, for the generation of photon pairs centered at 810 nm. The pump beam is spatially filtered and its optical power is controlled by a half-wave plate (HWP1) placed between two polarizers. Following the second polarizer, the pump power is monitored by means of a portion of the beam reflected by a coverslip, coupled into a multimode fiber, and detected by an avalanche photo diode (APD5). A second half-wave plate (HWP2) is used to adjust the polarization and optimize the SPDC generation rate, while the pump beam is brought to a focus on the plane of the nonlinear crystal [BBO1 (BBO2) for the collinear (noncollinear) configuration] using a 100 cm focal-length lens (L1). Note that a folding mirror (FM) allows the experimenter to choose between the collinear and noncollinear configurations, in such a way that the pump characteristics (spatial mode and optical power range) are identical in both cases.

In both configurations, pump suppression is achieved by transmitting the generated photon pairs through a composite filter (IF) comprised of (i) a long-pass filter (designed to transmit wavelengths $\lambda > 488$ nm) and (ii) a band-pass filter centered at 800 nm with a 40 nm width. Note that because in both configurations the unfiltered SPDC spectral width is much greater than 40 nm, the resulting filtered SPDC spectral width is defined solely by the filter bandwidth. In the collinear configuration (see Figure 1), the photon pairs are further transmitted through a telescope composed of lenses with focal lengths 10 and 3 cm (with an $M = 10/3$ magnification) and coupled, with the help of an aspheric-lens-based coupling system (CS1), into a multimode fiber which leads to the sample arm detection system (see below).

In the noncollinear configuration (see Figure 1), the signal and idler photons are reflected by two right-angle prism mirrors coated on their front surfaces for high reflectivity (PM), and in each resulting path, the corresponding photon is transmitted through a collimating lens with 10 cm focal length. While the idler photon is directly coupled into one of the single-mode input ports of a fiber-based beamsplitter (FBS1) using a coupling system (CS2), the horizontally polarized signal photon is transmitted through a polarizing beam splitter (PBS), and subjected to two passes through a quarter wave plate (QWP) so that the polarization is switched to vertical, and reflected from PBS on its return path. Note that the end mirror (EM) following QWP is mounted on a computer-controlled linear motor which permits the introduction of a controllable signal-idler temporal delay. Following its reflection from PBS, the signal photon is coupled into the other single-

https://doi.org/10.1021/acs.jpca.2c00720
J. Phys. Chem. A 2022, 126, 2185−2195

mode input port of FBS1 using a coupling system (CS3). The signal and idler photons (traveling in the single mode optical fibers) are each transmitted through a fiber polarization controller (FPC1 and FPC2) prior to being combined. On account of the Hong−Ou−Mandel (HOM) interference that occurs at the beamsplitter, at zero delay both photons emerge together through either of the two output ports (and they still emerge together half of the time for a large-delay setting). Note that one beamsplitter output is relayed, through coupling system CS4, into a multimode fiber which leads to the sample arm detection system (see below). The other, single-mode beamsplitter output is directed to the reference arm detection system (see below).

Our experimental design includes two separate detection systems, referred to as the sample and reference arms. While, in the former, the photon pairs are transmitted through the sample so that ETPA can take place, in the latter, the photon pairs are directly detected in coincidence in the absence of the sample, so that ETPA cannot take place. In the case of the sample arm, a stream of photon pairs conveyed through a multimode fiber is outcoupled into free space using coupling system CS5. Once in free space, the photon pairs are focused, using a 5 cm focal length lens, to a 122-μm-diameter spot. The sample, in the form of a molecular solution contained by a quartz cuvette of 1 cm length, is placed on the focal plane. The photon stream which emanates from the sample is collimated with the help of a second lens (with a 7.5 cm focal length), and is transmitted through a long-pass filter (LP) (designed to transmit wavelengths $\lambda > 750$ nm) in order to eliminate any fluorescence emitted by the sample. A beamsplitter (BS) then splits the photon pairs (nondeterministically) into two spatial modes and each output is coupled into a multimode fiber leading to an avalanche photodiode (APD1 and APD2). The electronic signals from APD1 and APD2 are recorded with the help of a time to digital converter (TDC), from which singles and coincicence rates are obtained.

In the case of the reference arm, the single-mode output of the HOM beamsplitter FBS1 is connected to one of the input ports of a second fiber-based beamsplitter (FBS2) which splits the photon pairs (nondeterministically). Each of the output ports of FBS2 leads to an avalanche photodiode (APD3 and APD4). As in the case of the sample arm, the electronic signals from APD3 and APD4 are recorded with the help of a time to digital converter, from which singles and coincidence rates are obtained. The reference arms allows us to monitor the expected ETPA behavior, in the sample arm, in comparison with an equivalent setup in which ETPA cannot occur.

It is important to note that the collinear configuration leads to a greater SPDC flux as compared to the noncollinear configuration because while, in the latter case, only a portion of the emission SPDC cone is utilized, in the former, in principle, all emitted photon pairs can participate. In addition, the simpler setup in the collinear configuration, with fewer optical elements, implies lower losses. For this reason, we take two types of measurement for the collinear configuration: (i) a flux-restricted measurement, in which the pump power is limited so that the resulting SPDC flux range matches the maximum flux range observed in the noncollinear configuration, thus allowing us to make direct comparisons between the two configurations, and (ii) a flux nonrestricted measurement for which the full available pump power is used resulting in a higher SPDC flux by 1 order of magnitude.

Importantly, apart from permitting the two detection systems discussed above, the noncollinear configuration also allows us to freely vary the signal-idler temporal delay τ. In our experimental work, we have used two particular delay settings: $\tau = 667$ fs (selected so that $|\tau| \gg T_e$, with T_e the entanglement time which in our case has a value of $T_e \approx 100$ fs; this value is obtained through HOM interference—see Supporting Information) as well as $\tau = 0$. The idea behind the use of these two delay settings is that they provide a useful experimental test: while we expect that ETPA can occur for the delay setting $\tau = 0$, ETPA clearly cannot occur for $\tau = 667$ fs, so that any apparent ETPA signal occurring for this latter delay value cannot be ascribed to ETPA. It is worth pointing out that due to group velocity dispersion (GVD), mainly occurring in our optical fibers, even in the zero delay setting only a limited percentage of the photon pairs arrive at the sample with $\tau = 0$ to within the entanglement time T_e, i.e. with $|\tau| < T_e/2$. In our case, considering the two meters of optical fiber (GVD = 35 fs^2/mm) used in our experiments, the percentage of pairs that arrive with zero delay is ∼3.7%. Note that this value is obtained by computing the overlap between the temporal shape of photon wave-packets with and without the effect of GVD, a method previously used in the context of ETPA measurements.[39,41]

We have performed ETPA experiments, based on the setup described above, for solutions of two organic compounds: (i) Rhodamine B (RhB) in methanol, and (ii) zinc tetraphenylporphyrin (ZnTPP) in toluene. In particular, we have used the following concentrations: 0.5, 1, 4.5, 10, and 58 mM for RhB and 1, 17, 120, 500, and 1400 μM for ZnTPP.

An experimental run consists of varying the pump power, using 12 distinct values as controlled by the motorized rotating half-wave plate HWP1, while the time to digital converter registers detection times for detectors APD1, APD2, and APD5 (collinear configuration), or for all detectors APD1-APD5 (noncollinear configuration). From these data, singles and coincidence counts may be extracted, while the effect of any pump power fluctuations can be compensated for through the signal from APD5 (see Supporting Information). Note that we have used a 7 ns coincidence window and an detection time of 1 s for each power value. The cycle of 12 measurements is repeated 45 times to obtain an average over 45 s per power value; while the experimental setup is thermally shielded, taking data in this manner minimizes the effect of temperature fluctuations which can mask the small flux differences through which ETPA is manifested. This procedure is repeated for the solvent and for each of the samples (defined by the organic compound and its concentration value). Note that in order to avoid optical deviation of the photon pairs which could likewise mask the effects under study, the cuvette is left in place, with the solution removed or inserted with a pipette as needed. The experimental procedure described above is carried out for each of the two configurations (collinear or noncollinear). In the collinear case, the procedure is completed twice, for each of the flux-restricted and flux nonrestricted measurements. In the noncollinear case, the procedure is likewise completed twice: for the zero delay ($\tau = 0$) and temporally delayed ($\tau = 667$ fs) settings. As already mentioned, while in the collinear case only the sample arm detection system can be used, in the noncollinear case data is taken concurrently with both detection systems (sample and reference arms).

https://doi.org/10.1021/acs.jpca.2c00720
J. Phys. Chem. A 2022, 126, 2185−2195

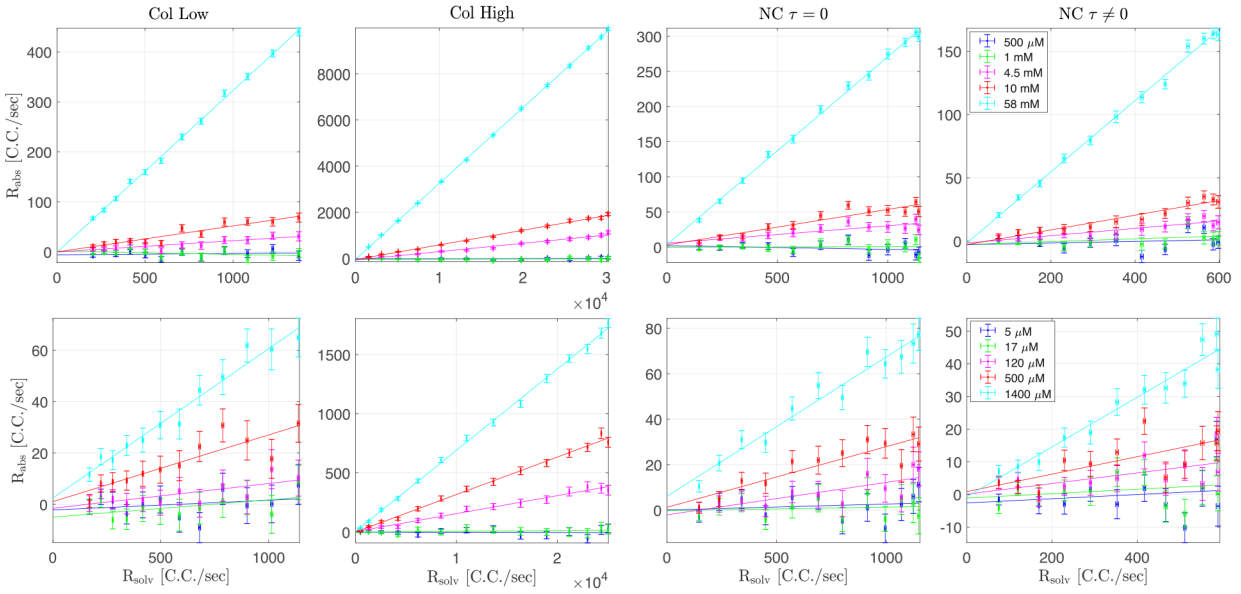

Figure 2. Absorption rates, quantified through coincidence counts, as a function of the incident photon-pair rates, for the four types of measurement: (i) collinear flux restricted, (ii) collinear flux nonrestricted, (iii) noncollinear with $\tau = 0$, and (iv) noncollinear with $\tau \neq 0$. Results are shown for five different concentration values of RhB (top row), and ZnTPP (lower row).

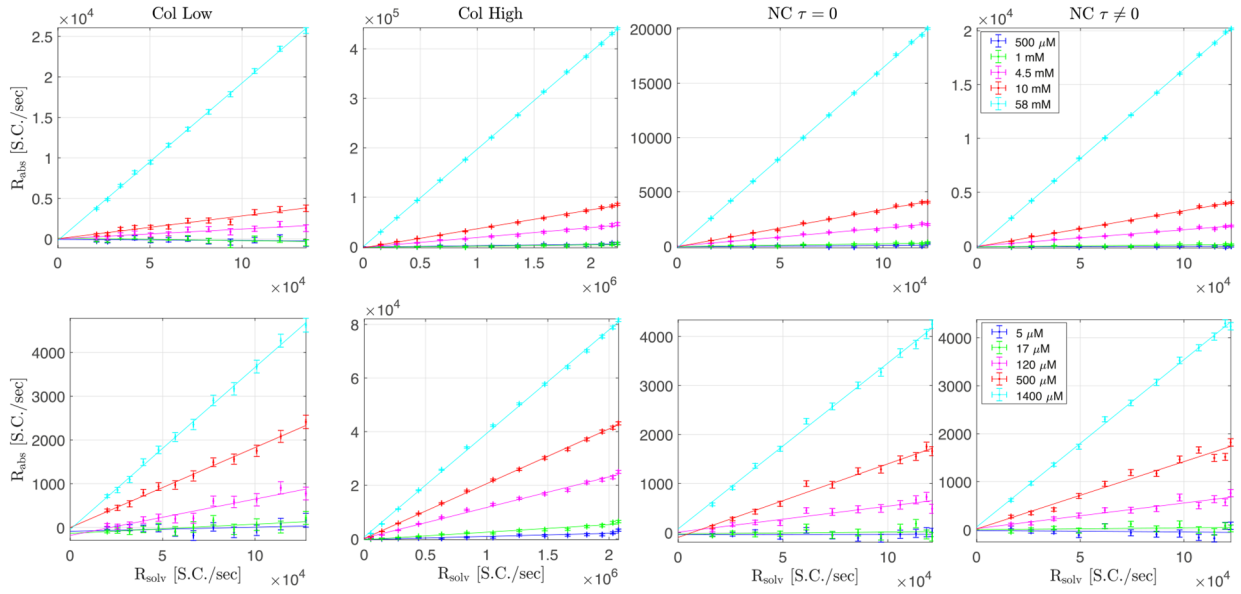

Figure 3. Absorption rates, quantified through singles counts, as a function of the incident photon-pair rates, for the four types of measurement: (i) collinear flux restricted, (ii) collinear flux nonrestricted, (iii) noncollinear with $\tau = 0$, and (iv) noncollinear with $\tau \neq 0$. Results are shown for five different concentration values of RhB (top row) and ZnTPP (lower row).

RESULTS AND DISCUSSION

As discussed in the Theory section, in order to experimentally determine the ETPA signal in molecular solutions, we can record the photon-pair rate reduction, R_{abs}, as a function of the incident photon-pair rate, as quantified by R_{solv}; note that this can be done either in terms of singles or coincidence counts. We have followed this strategy for our two configurations (collinear and noncollinear). On the one hand, for the collinear configuration we have carried out these measurements for the flux-restricted (in the figures below labeled as Col Low) and non-flux-restricted (Col High) cases. On the other hand, for the noncollinear configuration, we have carried out these measurements for the zero delay (labeled as NC $\tau = 0$) and nonzero delay (NC $\tau \neq 0$) settings.

Figures 2 and 3 show the results obtained for absorption rates in coincidences and singles counts, respectively. In both figures, the upper row corresponds to RhB while the lower row corresponds to ZnTPP. Each column shows one of the four possible types of measurements: (i) collinear flux-restricted, (ii) collinear non flux-restricted, (iii) noncollinear with $\tau = 0$, and (iv) noncollinear with $\tau = 667$ fs. Each panel shows five curves, one for each concentration, where the solid line represents a linear fit to the experimental points obtained as the average of the 45 1-s-duration measurements. The error bar indicates the standard-error of the mean calculated as $\sigma/$

https://doi.org/10.1021/acs.jpca.2c00720
J. Phys. Chem. A 2022, 126, 2185−2195

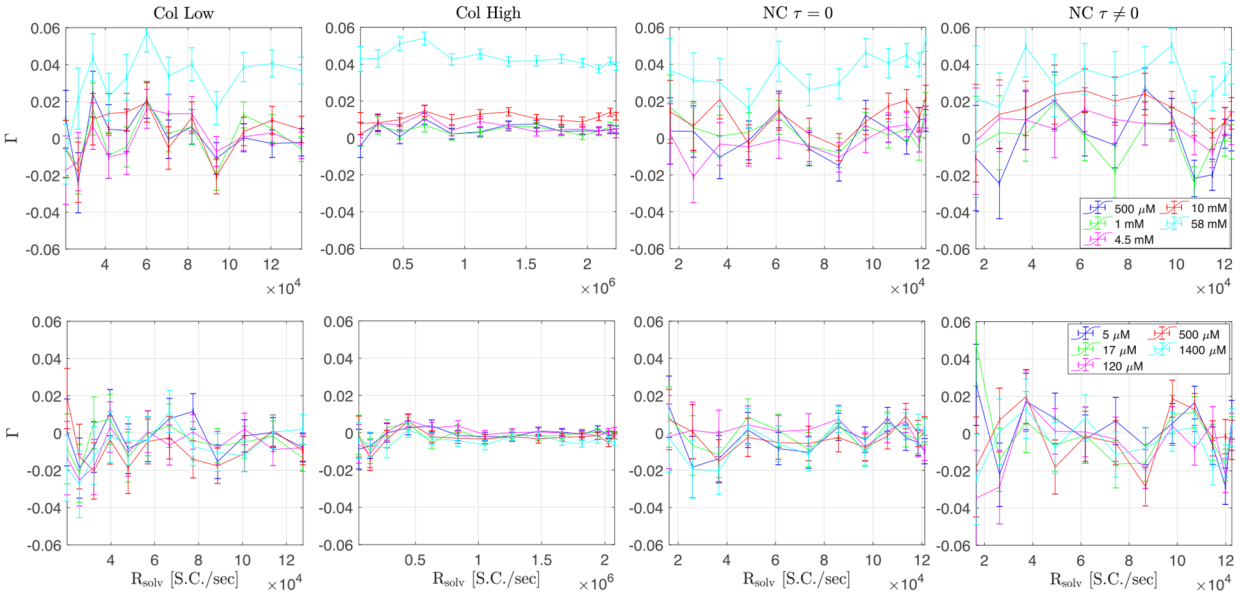

Figure 4. Γ value calculated from our experimental data (eq 9), as a function of the incident photon-pair rates, for the four types of measurement: (i) collinear flux restricted, (ii) collinear flux nonrestricted, (iii) noncollinear with $\tau = 0$, and (iv) noncollinear with $\tau \neq 0$. Results are shown for five different concentration values of RhB (top row) and ZnTPP (lower row).

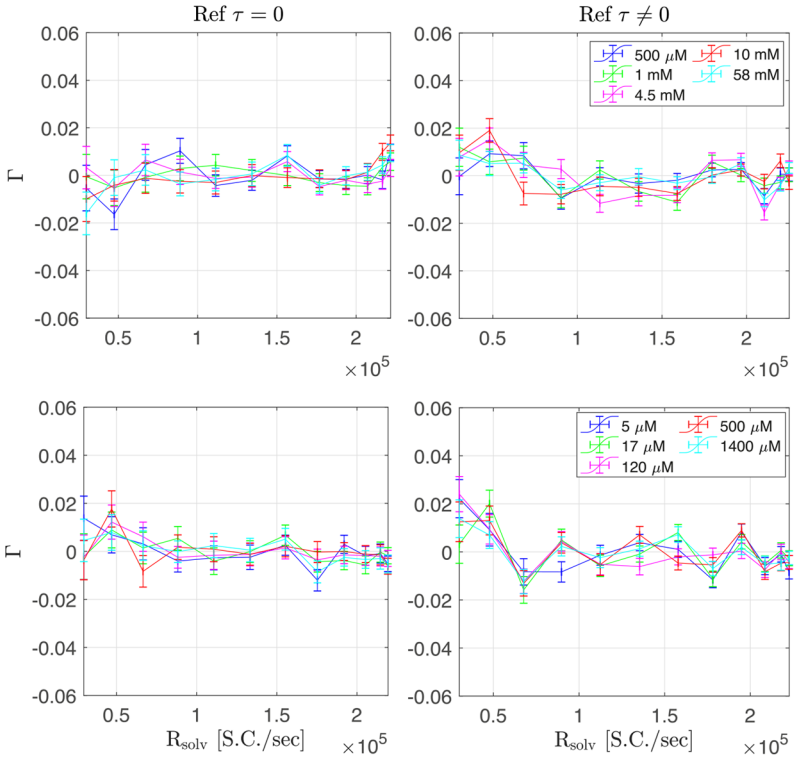

Figure 5. Γ value calculated from the reference-arm experimental data in the noncollinear configuration ($\tau = 0$ in the first column and $\tau \neq 0$ in the second column). Results are shown for five different concentration values of RhB (top row) and ZnTPP (lower row).

$\sqrt{n}$ where σ is the standard deviation among the $n = 45$ measurements.

Note that all curves have a linear behavior, as expected from Equation 3, with a slope that grows monotonically with the concentration. Note also that for a given sample and concentration value, the slope values are not only of the same order of magnitude but in fact are very similar to each other, across the four types of measurements. For the collinear configuration, this would indicate that for a R_{solv} ranging from around 200 to 3×10^4 coincidences per second, the absorption rate is characterized by a linear behavior (see the first two columns of Figure 2). The same goes for singles counts, as it is observed that for a R_{solv} ranging from 2×10^4 to 2×10^6 counts per second the trend is also linear. Surprisingly, when analyzing the behavior of the last column, it can be seen that neither for RhB nor for ZnTPP is the absorption signal suppressed as

https://doi.org/10.1021/acs.jpca.2c00720
J. Phys. Chem. A 2022, 126, 2185−2195

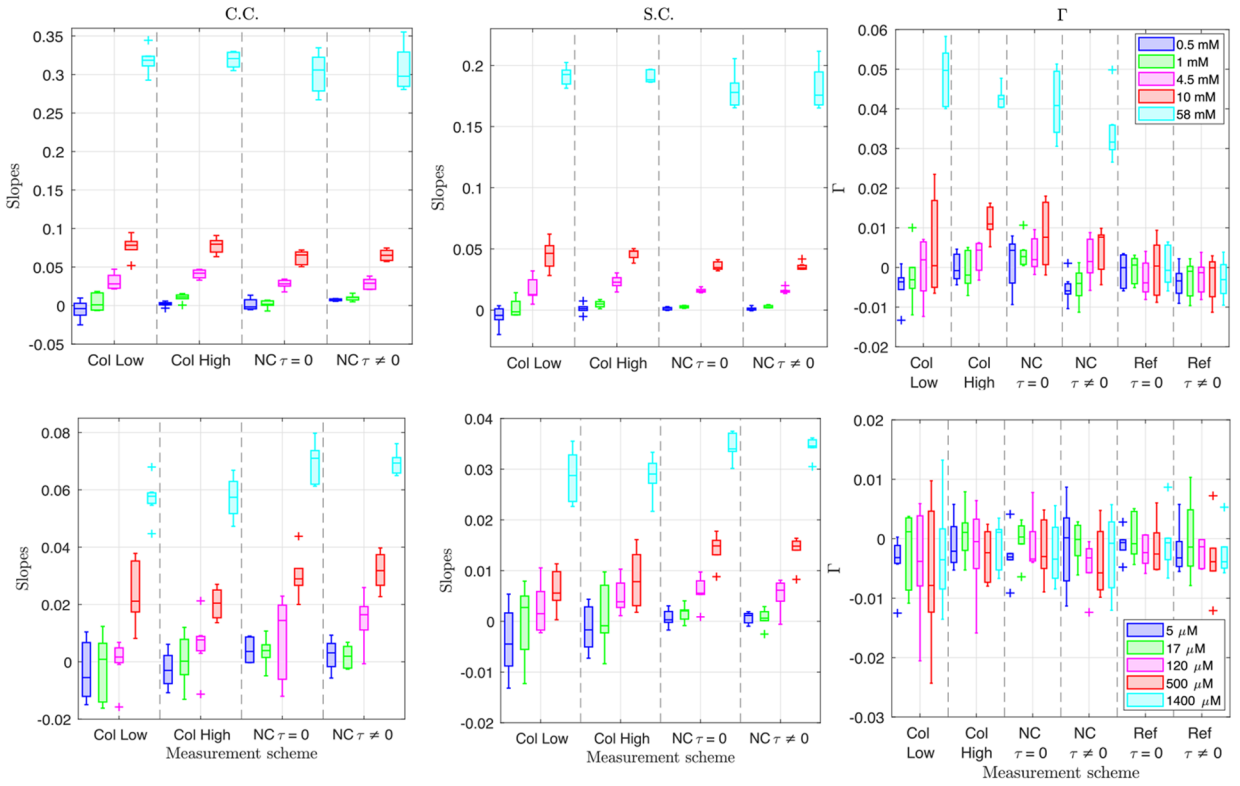

Figure 6. Graphical summary of all measurements taken in our experiment, with RhB in the first row and ZnTPP in the second row. The first [second] column shows the slope of the R_{abs} vs R_{solv} curves (in terms of coincidence [singles] counts). The third column shows the values for Γ obtained from our experimental data. In each panel there is a block for each type of measurement (collinear flux restricted, collinear flux nonrestricted, noncollinear with $\tau = 0$, and noncollinear with $\tau \neq 0$); in the case of the third column, two additional types of measurement are included: reference arm with $\tau = 0$ and $\tau \neq 0$. A boxplot, colored according to the concentration, represents the spread of slopes or Γ values obtained for independent measurements x.

expected when the condition $|\tau| \gg T_e$ is fulfilled, i.e., a linear absorption vs incident photon rate behavior with a slope that increases monotonically with the concentration value is still observed. Moreover, the slopes obtained for the $\tau = 0$ and $|\tau| \gg T_e$ cases have very similar values. Note that while the behavior shown in these figures is similar to that reported previously by other groups, the fact that the absorption is not suppressed for the large-delay setting implies that, actually, the observed behavior cannot be attributed to ETPA. The characteristics apparent in our results (linear behavior with a slope which increases monotonically with concentration; see Figures 2 and 3), may in fact be due to the presence of other, linear, contributions. In order to eliminate such linear contributions from our data, and retain only the signal from two-photon processes, we calculate Γ using eq 9.

The values for Γ that we obtain from our experimental data are shown in Figure 4, plotted vs the incident photon rates on the sample. The results for RhB are shown in the upper row, whereas those for ZnTPP are shown in the lower row. Note that in this type of plot, the presence of ETPA would be consistent with a constant value of Γ (with respect to the incident photon rate), which increases with the concentration, since $\Gamma = \overline{R}^{(2)}_{abs} / \overline{R}^{(2)}_{solv}$ represents the fraction of biphotons absorbed from the total available. It is apparent from the Figure 4 that in the case of higher photon rates (see particularly the second column), the error bars are smaller, because of the reduced fluctuations in singles and coincidence counts. It can be observed that for ZnTPP the curves for all concentrations are grouped around Γ = 0, regardless of the type of measurement (each corresponding to one of the columns). This indicates that the results for ZnTPP shown in Figures 2 and 3 are due exclusively to linear losses and not to two-photon losses, which reinforces the argument that they cannot be attributed to ETPA. A similar behavior is observed for RhB, with the curves for the lower concentrations again largely grouped around Γ = 0. However, for the higher concentrations (particularly for 58 mM), Γ fluctuates around nonzero values. Note that this is the case for all types of measurement, with Γ values clearly separated from those corresponding to lower concentrations. Although this effect probably represents a two-photon process, it does not exhibit all of the expected characteristics of ETPA. In particular, as can be seen in Figure 4, the signal is not suppressed for $\tau = 667$ fs, as would have to be the case for ETPA.

As mentioned above, one of the key features of our experimental setup is that it includes a reference arm, which is equivalent to the sample arm except that there is no sample present. Thus, while running the absorption experiments in the various samples with different concentrations, the behavior of the signal is also recorded for the reference arm. Because data are taken concurrently in both the sample and reference arms, we may plot in the reference-arm a Γ vs incident counts curve, corresponding to each such sample-arm plot, as if absorption were taking place in the reference arm; see Figure 5. Note that the color code represents the concentration of the sample, in the sample arm.

The absence of a sample in the reference arm implies that there cannot be any two-photon losses, so that we expect that

https://doi.org/10.1021/acs.jpca.2c00720
J. Phys. Chem. A 2022, 126, 2185−2195

Table 1. Apparent ETPA Cross Section for All RhB Concentrations Calculated through Equation 3, in Coincidences, for All Four Types of Experiment

	$\sigma_E \times 10^{-21}$ [cm^2/molecule]			
c (mM)	Col Low	Col High	$\tau = 0$	$\tau = 667$ fs
0.5	18.150(42.703)	6.468(10.256)	4.508(24.466)	24.248(4.612)
1	6.663(18.404)	16.814(8.788)	3.031(7.933)	16.243(5.965)
4.5	11.478(3.921)	15.132(2.173)	10.390(2.194)	10.411(2.688)
10	12.699(2.449)	12.933(1.774)	10.342(1.574)	10.848(1.302)
58	9.107(0.668)	8.136(0.538)	8.643(0.844)	8.832(0.914)

Table 2. Apparent ETPA Cross Section for All ZnTPP Concentrations Calculated through Equation 3 with Coincidences Measurements, for All Four Types of Experiment[a]

	$\sigma_E \times 10^{-19}$ [cm^2/molecule]			
c (mM)	Col Low	Col High	$\tau = 0$	$\tau = 667$ fs
5	–	–	13.490(13.693)	8.117(18.528)
17	–	0.358(8.462)	3.461(5.115)	1.849(4.021)
120	0.0432(1.040)	0.877(1.334)	1.231(1.993)	2.041(1.243)
500	0.813(0.366)	0.683(0.179)	1.001(0.269)	1.052(0.242)
1400	0.676(0.088)	0.680(0.0901)	0.827(0.093)	0.823(0.063)

[a]Cases where a value is not displayed have been omitted on account of yielding a negative effective section; however, when considering the error, they are all consistent with a positive cross-section.

all curves should be grouped around $\Gamma = 0$. Our results (Figure 5) show this expected behavior for all concentration values of both RhB and ZnTPP. Note that these results also showcase the excellent stability of our setup: fluctuations are kept low enough so that the value of Γ remains stable. Note also that the departure from $\Gamma = 0$ observed for higher concentrations of RhB in the sample arm is not observed for the reference arm.

Generally speaking, transmission-based ETPA experiments can be challenging because the measured effects hinge upon small differences in the resulting count rate with and without the sample in place. Photon counting naturally presents fluctuations which must be made as small as possible so as to obtain meaningful results. In this context, so as to assess our experimental reproducibility, Figure 6 shows a graphical summary across all our types of measurement, with the upper row corresponding to RhB and the lower row to ZnTPP. The first column shows the slope of the R_{abs} vs R_{solv} curves (in terms of coincidence counts; see Figure 2). In each panel, there are four blocks, each corresponding to a type of measurement: (i) collinear flux-restricted, (ii) collinear non flux-restricted, (iii) noncollinear with $\tau = 0$, and (iv) noncollinear with $\tau = 667$ fs. Within each block, a boxplot (colored according to the concentration value) represents the spread of slope values obtained among six or seven independent measurements, so that all measurements are contained between the error bars of the graph, except outliers marked with "+" symbols (which significantly depart from the group trend). The median is represented by the horizontal line within each box, while the lower and upper box edges represent the lower and upper distribution quartiles. The second column is similar to the first except that it is based on slope values of R_{abs} vs R_{solv} curves obtained from singles, rather than coincidence, counts; see Figure 3. The third column shows the values for Γ obtained across all types of experiment, also including data corresponding to the reference arm, for both $\tau = 0$ and $\tau = 667$ fs.

From an analysis of Figure 6, it becomes apparent that, within the fluctuations of the experiment, the results are remarkably repeatable. While in the case of the two leftmost columns, the slope values increase monotonically with the concentration, in the rightmost column the Γ values group around 0 for all concentrations of ZnTPP, as well as for the lower concentrations of RhB. Note that for a given sample and concentration value, the obtained slopes (see the two leftmost columns) have remarkably similar values across all four types of measurements.

As previously discussed, we conclude that despite the reproducibility of these results, because the purported ETPA signal occurs for $|\tau| \gg T_e$ (and is very similar to that obtained for $\tau = 0$), it in fact cannot be attributed to ETPA. Recent experimental work has pointed out that this type of behavior might be due to one-photon loss mechanisms, such as hot-band absorption,[50] that could mimic ETPA. We believe this type discussion will motivate future investigations toward finding single-photon-loss-independent metrics (or witnesses) for ETPA, such as our own analysis in terms of the Γ quantity [see eq 9] which is indeed linear-loss-independent.

In addition, as we previously stated, our results help to conclude that for the higher concentrations of RhB there is an apparent two-photon loss mechanism, which likewise cannot be attributed to ETPA. One could argue that this spurious signal might be a result of high-concentration molecular aggregation,[25] that creates low-lying energy levels, from which one-photon absorption events may take place. We are certain that this discussion will trigger new investigations on the role of molecular aggregation in ETPA experiments.

Finally, although we conclude that the results which we obtain do not originate from the ETPA process, we have calculated the *apparent* ETPA-cross section values, as obtained from eq 3; these values are shown in Tables 1 and 2, for RhB and ZnTPP, respectively. Note that these values are of the same orders of magnitude as compared to those previously reported by other groups. Moreover, they are within the bounds established by eq 6, i.e., for RhB on the order of 10^{-21} cm^2/molecule and for ZnTPP on the order of 10^{-19} cm^2/molecule.

https://doi.org/10.1021/acs.jpca.2c00720
J. Phys. Chem. A 2022, 126, 2185−2195

CONCLUSIONS

We have presented a new method for the estimation of the entangled two-photon absorption (ETPA) rate in a transmission-based experiment. Unlike the standard scheme based on the slope of the absorption (obtained by switching between sample and solvent) vs the incident photon-pair rates, quantified either in coincidence or singles counts, our method relies on taking into account both singles and coincidences and works irrespective of any linear loss mechanisms and/or any intrinsic dependence of the photon-pair flux on the signal-idler temporal delay introduced. Our experimental design includes two different configurations: based either on a collinear or noncollinear SPDC source, in both of which we can vary the photon-pair flux and the sample concentration. The noncollinear configuration additionally permits the introduction of a controllable signal-idler temporal delay and also permits two distinct detection systems, the sample and reference arms, the second differing from the first in that an ETPA sample is not present. Because the photon-pair streams reaching the two detection systems (which are obtained from the two output ports of a Hong−Ou−Mandel interferomer) are equivalent, the reference arm acts as a useful control to assess the behavior of the sample arm.

We find that our own measurements carried out in the standard scheme are compatible with those obtained previously by other authors, with apparent ETPA cross sections fulfilling the bound established in eq 6. We nevertheless also find through our noncollinear configuration that (i) the ETPA signal is not suppressed for temporal delays τ greater than the photon-pair characteristic correlation time T_e, i.e., $|\tau| \gg T_e$, and (ii) the two-photon absorption signal obtained through our method, Γ, is not appreciably different between the sample and reference arms, except at higher concentrations of RhB (particularly 58 mM), for which a two-photon signal is obtained, which however is not suppressed for $|\tau| \gg T_e$. In view of these findings, it is fair to conclude that the transmission-based methods that are currently employed to explore ETPA are not entirely reliable. Our work and that presented by Li et al.,[34] in which only a 40 times enhancement of the absorption signal was reported (despite using large fluxes of strongly correlated photons), suggest that the available flux of entangled photons in our work and several others with similar photon-pair flux levels is insufficient to produce an ETPA signal that is strong enough to be distinguished from other effects such as linear absorption and scattering. Alternatively, the cross sections of these molecules could be inaccessible through a transmission-based method, which is in agreement with the work presented by Parzuchowski et al.[39] We believe that our work will shed light on the current debate regarding the viability of the transmission-based scheme for ETPA in organic compounds.

ASSOCIATED CONTENT

Supporting Information

The Supporting Information is available free of charge at https://pubs.acs.org/doi/10.1021/acs.jpca.2c00720.

Additional experimental details and methods explaining the mechanism for the controlled temporal delay and the method for the reference-based error estimation (PDF)

AUTHOR INFORMATION

Corresponding Authors

Roberto de J. León-Montiel − *Instituto de Ciencias Nucleares, Universidad Nacional Autonoma de México, 04510 Ciudad de México, México;* orcid.org/0000-0002-3045-3604; Email: roberto.leon@nucleares.unam.mx

Alfred B. U'Ren − *Instituto de Ciencias Nucleares, Universidad Nacional Autonoma de México, 04510 Ciudad de México, México*; Email: alfred.uren@nucleares.unam.mx

Authors

Samuel Corona-Aquino − *Instituto de Ciencias Nucleares, Universidad Nacional Autonoma de México, 04510 Ciudad de México, México;* orcid.org/0000-0003-2988-4930

Omar Calderón-Losada − *Instituto de Ciencias Nucleares, Universidad Nacional Autonoma de México, 04510 Ciudad de México, México*

Mayte Y. Li-Gómez − *Instituto de Ciencias Nucleares, Universidad Nacional Autonoma de México, 04510 Ciudad de México, México*

Hector Cruz-Ramirez − *Instituto de Ciencias Nucleares, Universidad Nacional Autonoma de México, 04510 Ciudad de México, México*

Violeta Álvarez-Venicio − *Instituto de Ciencias Nucleares, Universidad Nacional Autonoma de México, 04510 Ciudad de México, México*

María del Pilar Carreón-Castro − *Instituto de Ciencias Nucleares, Universidad Nacional Autonoma de México, 04510 Ciudad de México, México*

Complete contact information is available at: https://pubs.acs.org/10.1021/acs.jpca.2c00720

Notes

The authors declare no competing financial interest.

ACKNOWLEDGMENTS

R.d.J.L.-M. thankfully acknowledges financial support by CONACyT under Project CB-2016-01/284372 and by DGAPA-UNAM under Project UNAM-PAPIIT IN102920. A.B.U. thankfully acknowledges support from AFOSR Grant FA9550-21-1-0147, from UNAM-PAPIIT Grant IN103521, and from CONACyT Grant 217559. S.C.-A thankfully acknowledges CONACyT for the master scholarship. V.A-V. acknowledges CONACyT for the Cátedra 411-2016. M.d.P.C.-C. thankfully acknowledges support from DGAPA-PAPIIT IN207421.

REFERENCES

(1) Denk, W.; Strickler, J. H.; Webb, W. W. Two-Photon Laser Scanning Fluorescence Microscopy. *Science* **1990**, *248*, 73−76.

(2) Xu, C.; Webb, W. W. Measurement of two-photon excitation cross sections of molecular fluorophores with data from 690 to 1050 nm. *J. Opt. Soc. Am. B* **1996**, *13*, 481.

(3) Rumi, M.; Perry, J. W. Two-photon absorption: an overview of measurements and principles. *Adv. Opt. Photon.* **2010**, *2*, 451.

(4) Pastirk, I.; Cruz, J. M. D.; Walowicz, K. A.; Lozovoy, V. V.; Dantus, M. Selective two-photon microscopy with shaped femtosecond pulses. *Opt. Express* **2003**, *11*, 1695−1701.

(5) Choi, H.; So, P. T. C. Improving femtosecond laser pulse delivery through a hollow core photonic crystal fiber for temporally focused two-photon endomicroscopy. *Sci. Rep.* **2015**, *4*, 6626.

(6) Patterson, G. H.; Piston, D. W. Photobleaching in two-photon excitation microscopy. *Biophys. J.* **2000**, *78*, 2159−62.

(7) Podgorski, K.; Ranganathan, G. Brain heating induced by near-infrared lasers during multiphoton microscopy. *J. Neurophysiol* **2016**, *116*, 1012−1023.
(8) Javanainen, J.; Gould, P. L. Linear intensity dependence of a two-photon transition rate. *Phys. Rev. A* **1990**, *41*, 5088−5091.
(9) Fei, H.-B.; Jost, B. M.; Popescu, S.; Saleh, B. E. A.; Teich, M. C. Entanglement-Induced Two-Photon Transparency. *Phys. Rev. Lett.* **1997**, *78*, 1679.
(10) Lee, D. I.; Goodson, T. Entangled Photon Absorption in an Organic Porphyrin Dendrimer. *J. Phys. Chem. B* **2006**, *110*, 25582.
(11) Roslyak, O.; Mukamel, S. Multidimensional pump-probe spectroscopy with entangled twin-photon states. *Phys. Rev. A* **2009**, *79*, 063409.
(12) Roslyak, O.; Marx, C. A.; Mukamel, S. Nonlinear spectroscopy with entangled photons: Manipulating quantum pathways of matter. *Phys. Rev. A* **2009**, *79*, 033832.
(13) Guzman, A. R.; Harpham, M. R.; Süzer, Ö.; Haley, M. M.; Goodson, T. G. Spatial Control of Entangled Two-Photon Absorption with Organic Chromophores. *J. Am. Chem. Soc.* **2010**, *132*, 7840.
(14) Raymer, M. G.; Marcus, A. H.; Widom, J. R.; Vitullo, D. L. P. Entangled photon-pair two-dimensional fluorescence spectroscopy (EPP-2DFS). *J. Phys. Chem. B* **2013**, *117*, 15559.
(15) Schlawin, F.; Dorfman, K. E.; Fingerhut, B. P.; Mukamel, S. Suppression of population transport and control of exciton distributions by entangled photons. *Nat. Commun.* **2013**, *4*, 1782.
(16) Schlawin, F.; Dorfman, K. E.; Mukamel, S. Pump-probe spectroscopy using quantum light with two-photon coincidence detection. *Phys. Rev. A* **2016**, *93*, 023807.
(17) Saleh, B. E. A.; Jost, B. M.; Fei, H.-B.; Teich, M. C. Entangled-Photon Virtual-State Spectroscopy. *Phys. Rev. Lett.* **1998**, *80*, 3483.
(18) Kojima, J.; Nguyen, Q.-V. Entangled biphoton virtual-state spectroscopy of the $A^2\Sigma^+-\chi^2\Pi$ system of OH. *chem phys lett* **2004**, *396*, 323.
(19) Peřina, J.; Saleh, B. E. A.; Teich, M. C. Multiphoton absorption cross section and virtual-state spectroscopy for the entangled *n*-photon state. *Phys. Rev. A* **1998**, *57*, 3972.
(20) León-Montiel, R. de J.; Svozilík, J.; Salazar-Serrano, L. J.; Torres, J. P. Role of the spectral shape of quantum correlations in two-photon virtual-state spectroscopy. *New J. Phys.* **2013**, *15*, 053023.
(21) Dorfman, K. E.; Schlawin, F.; Mukamel, S. Nonlinear optical signals and spectroscopy with quantum light. *Rev. Mod. Phys.* **2016**, *88*, 045008.
(22) Schlawin, F. Entangled photon spectroscopy. *J. Phys. B: At. Mol. Opt. Phys.* **2017**, *50*, 203001.
(23) Oka, H. Efficient selective two-photon excitation by tailored quantum-correlated photons. *Phys. Rev. A* **2010**, *81*, 063819.
(24) Schlawin, F.; Dorfman, K. E.; Mukamel, S. Entangled Two-Photon Absorption Spectroscopy. *Acc. Chem. Res.* **2018**, *51*, 2207.
(25) Villabona-Monsalve, J. P.; Calderón-Losada, O.; Nũnez Portela, M.; Valencia, A. Entangled Two Photon Absorption Cross Section on the 808 nm Region for the Common Dyes Zinc Tetraphenylporphyrin and Rhodamine B. *J. Phys. Chem. A* **2017**, *121*, 7869−7875.
(26) Varnavski, O.; Pinsky, B.; Goodson, T. Entangled Photon Excited Fluorescence in Organic Materials: An Ultrafast Coincidence Detector. *J. Phys. Chem. Lett.* **2017**, *8*, 388.
(27) Oka, H. Enhanced vibrational-mode-selective two-step excitation using ultrabroadband frequency-entangled photons. *Phys. Rev. A* **2018**, *97*, 063859.
(28) Oka, H. Two-photon absorption by spectrally shaped entangled photons. *Phys. Rev. A* **2018**, *97*, 033814.
(29) Svozilík, J.; Peřina, J.; León-Montiel, R. de J. Virtual-state spectroscopy with frequency-tailored intense entangled beams. *J. Opt. Soc. Am. B* **2018**, *35*, 460.
(30) Svozilík, J.; Peřina, J.; León-Montiel, R. de J. Two-photon absorption spectroscopy using intense phase-chirped entangled beams. *Chem. Phys.* **2018**, *510*, 54.
(31) Burdick, R. K.; Varnavski, O.; Molina, A.; Upton, L.; Zimmerman, P.; Goodson, T. Predicting and Controlling Entangled Two-Photon Absorption in Diatomic Molecules. *J. Phys. Chem. A* **2018**, *122*, 8198−8212.
(32) León-Montiel, R. de J.; Svozilík, J.; Torres, J. P.; U'Ren, A. B. Temperature-Controlled Entangled-Photon Absorption Spectroscopy. *Phys. Rev. Lett.* **2019**, *123*, 023601.
(33) Harpham, M. R.; Süzer, Ö.; Ma, C. Q.; Bäuerle, P.; Goodson, T. Thiophene Dendrimers as Entangled Photon Sensor Materials. *J. Am. Chem. Soc.* **2009**, *131*, 973.
(34) Li, T.; Li, F.; Altuzarra, C.; Classen, A.; Agarwal, G. S. Squeezed Light Induced Two-Photon Absorption Fluorescence of Fluorescein Biomarkers. *Appl. Phys. Lett.* **2020**, *116*, 254001.
(35) Landes, T.; Raymer, M. G.; Allgaier, M.; Merkouche, S.; Smith, B. J.; Marcus, A. H. Quantifying the enhancement of two-photon absorption due to spectral-temporal entanglement. *Opt. Express* **2021**, *29*, 20022−20033.
(36) Upton, L.; Harpham, M.; Suzer, O.; Richter, M.; Mukamel, S.; Goodson, T. Optically Excited Entangled States in Organic Molecules Illuminate the Dark. *J. Phys. Chem. Lett.* **2013**, *4*, 2046−2052.
(37) Villabona-Monsalve, J. P.; Varnavski, O.; Palfey, B. A.; Goodson, T. Two-Photon Excitation of Flavins and Flavoproteins with Classical and Quantum Light. *J. Am. Chem. Soc.* **2018**, *140*, 14562−14566.
(38) Eshun, A.; Cai, Z.; Awies, M.; Yu, L.; Goodson, T. Investigations of Thienoacene Molecules for Classical and Entangled Two-Photon Absorption. *J. Phys. Chem. A* **2018**, *122*, 8167.
(39) Parzuchowski, K. M.; Mikhaylov, A.; Mazurek, M. D.; Wilson, R. N.; Lum, D. J.; Gerrits, T.; Camp, C. H.; Stevens, M. J.; Jimenez, R. Setting limits on two-photon absorption cross sections in common fluorescent molecules with entangled photon pairs excitation. *Phys. Rev. Applied* **2021**, *15*, 044012.
(40) Hickam, B. P.; He, M.; Szoke, S.; Cushing, S. Measurement of Entangled State before, during, and after a Proposed Entangled Two-Photon Molecular Excitation. *arXiv* 2022; 2202.11764.
(41) Tabakaev, D.; Montagnese, M.; Haack, G.; Bonacina, L.; Wolf, J.-P.; Zbinden, H.; Thew, R. T. Energy-time-entangled two-photon molecular absorption. *Phys. Rev. A* **2021**, *103*, 033701.
(42) Landes, T.; Allgaier, M.; Merkouche, S.; Smith, B. J.; Marcus, A. H.; Raymer, M. G. Experimental feasibility of molecular two-photon absorption with isolated time-frequency-entangled photon pairs. *Phys. Rev. Res.* **2021**, *3*, 033154.
(43) Varnavski, O.; Goodson, T. Two-Photon Fluorescence Microscopy at Extremely Low Excitation Intensity: The Power of Quantum Correlations. *J. Am. Chem. Soc.* **2020**, *142*, 12966.
(44) Mikhaylov, A.; Parzuchowski, K. M.; Mazurek, M. D.; Lum, D. J.; Gerrits, T., Jr.; Champ, C. H.; Stevens, M. J.; Jimenez, R. A comprehensive experimental system for measuring molecular two-photon absorption using an ultrafast entangled photon pair excitation source. *Proc. SPIE 11295, Advanced Optical Techniques for Quantum Information, Sensing, and Metrology* **2020**, *11295*, 23.
(45) Lavoie, J.; Landes, T.; Tamimi, A.; Smith, B. J.; Marcus, A. H.; Raymer, M. G. Phase-Modulated Interferometry, Spectroscopy and Refractometry using Entangled Photon-Pairs. *Adv. Quantum Technol.* **2020**, *3*, 1900114.
(46) Shih, Y. Entangled biphoton source - property and preparation. *Rep. Prog. Phys.* **2003**, *66*, 1009.
(47) Kurtsiefer, C.; Oberparleiter, M.; Weinfurter, H. High-efficiency entangled photon pair collection in type-II parametric fluorescence. *Phys. Rev. A* **2001**, *64*, 023802.
(48) Süzer, Ö; Goodson, T. G., III Does pump beam intensity affect the efficiency of spontaneous parametric down conversion? *Opt. Express* **2008**, *16*, 20166.
(49) Schneeloch, J.; Knarr, S. H.; Bogorin, D. F.; Levangie, M. L.; Tison, C. C.; Frank, R.; Howland, G. A.; Fanto, M. L.; Alsing, P. M. Introduction to the absolute brightness and number statistics in spontaneous parametric down-conversion. *J. Opt* **2019**, *21*, 043501.
(50) Mikhaylov, A.; Wilson, R. N.; Parzuchowski, K. M.; Mazurek, M. D.; Camp, C. H.; Stevens, M. J.; Jimenez, R. Hot-Band Absorption Can Mimic Entangled Two-Photon Absorption. *J. Phys. Chem. Lett.* **2022**, *13*, 1489−1493.

https://doi.org/10.1021/acs.jpca.2c00720
J. Phys. Chem. A 2022, 126, 2185−2195